Journal of Geophysical Research - Planets

Supporting Information for

Seasonal variations in atmospheric composition as measured in Gale Crater, Mars

Melissa G. Trainer[1*], Michael H. Wong[2], Timothy H. McConnochie[3], Heather B. Franz[1], Sushil K. Atreya[2], Pamela G. Conrad[4], Franck Lefèvre[5], Paul R. Mahaffy[1], Charles A. Malespin[1], Heidi L. K. Manning[6], Javier Martín-Torres[7,8], Germán M. Martínez[9,2], Christopher P. McKay[10], Rafael Navarro-González[11], Álvaro Vicente-Retortillo[2], Christopher R. Webster[12], María-Paz Zorzano[13, 7]

[1]NASA Goddard Space Flight Center (GSFC), Greenbelt, MD; [2]University of Michigan, Ann Arbor, MI ; [3]University of Maryland, College Park, MD ; [4]Geophysical Laboratory, Carnegie Institution of Washington, Washington, DC; [5]LATMOS, CNRS, Sorbonne Université, UVSQ, Paris, France; [6]Misericordia University, Dallas PA 18612; [7]Division of Space Technology, Department of Computer Science, Electrical and Space Engineering, Luleå University of Technology, Luleå, Sweden; [8]Instituto Andaluz de Ciencias de la Tierra (CSIC-UGR), Granada, Spain; [9]Lunar and Planetary Institute, Universities Space Research Association, Houston, TX; [10] NASA Ames Research Center, Moffett Field, CA; [11] Instituto de Ciencias Nucleares. Universidad Nacional Autónoma de México, Ciudad de México,, Mexico; [12] NASA Jet Propulsion Laboratory, California Institute of Technology, Pasadena, CA; [13]Centro de Astrobiología (INTA-CSIC), Torrejón de Ardoz, Madrid, Spain

Contents of this file

1. Volume Mixing Ratios of major components on Mars.

Table S1. Instantaneous volume mixing ratios measured on Mars as measured by the SAM QMS, and as shown in Figures 5, 6, 7, 10, and 12. *Uploaded as: trainer_table_S1.xlsx*

Averaged instantaneous mixing ratios are provided for experiments in which there are two separate ingests (TIDs 25027 - 25337, inclusive). Integer Sol and L_s values indicate the timing for the first ingestion in these cases. Higher resolution Sol and L_s values are provided for each ingest in Table 1 in the main text. As discussed in the text (§2.1.1) the uncertainties on the reported CO_2 mixing ratios were computed relative to the trace gases, rather than propagated from the calibration constants [*Franz et al.*, 2017]. This was done to reflect the natural constraint that the VMR values must sum to 1, and therefore the uncertainty on the CO_2 mixing ratio should not exceed the sum of the uncertainties on the other species. It is important to note, however, that calculations of the partial pressures of CO_2 from these mixing ratio data must include the 3% uncertainty largely imposed by the uncertainty on the calibration constant. These data are also available at a free online data repository [*Trainer*, 2019].

2. Derivation of annual global mean pressure correction.

The mean daily pressure at a given season (L_s) is controlled by the global CO_2 budget and is driven by the seasonal CO_2 cycle. Daily pressure variations of up to 1.4 mbar have been observed, but these are assumed to be tidal and therefore do not affect the composition [*Martínez et al.*, 2017]. The absolute magnitude of the surface pressure also varies with altitude, which is important for comparisons between landing sites or during the mission as Curiosity has moved up the flanks of Mt. Sharp. The change in daily mean pressure throughout the Mars year is attributed to the addition and removal of CO_2 from the atmosphere, and therefore the instantaneous mixing ratio of any non-condensable, long-lived species is also changing as a function of L_s. Mixing ratios for the non-condensable species taken at different times of the martian year and locations on Mars should be corrected to the annual mean mixing ratio prior to direct comparison to account for these known variations [most recently demonstrated in *Krasnopolsky*, 2017].

The REMS daily average pressure data for MSL sols 10 – 1870 are shown in Figure S1. The data were fit with a polynomial and binned to integer L_s values. The fitted pressure vs. Ls was divided by the annual average pressure to generate the correction factor (F_P) used to calculate the annual average VMR values:

$$F_P = P_{atm}(t)/P_{avg} \quad \text{(S1).}$$

The derived F_P correction values are provided in Table S2.

During the time the atmospheric mixing ratio measurements were made, the rover has climbed approximately 350 m, creating the small decrease in the absolute pressure, as seen by the shaded dots in Figure S1. The steepest change in elevation occurs after sol 1357, going from an average climb rate of 0.09 m/sol to 0.5 m/sol after this sol. Therefore, the mixing ratios measured in the latter half of MY 33 and MY 34 were from an increasingly thinning atmosphere, with a relative decrease of 3% of the atmospheric pressure at landing. Thus, the pressure correction shown as the red trace in Figure S1 is weighted toward the first two years of data, when the elevation (and therefore pressure) change was minor. The correction is then applied as a function of the L_s value, not the ambient pressure at the time of the experiment. Thus, the change in elevation and ambient pressure does not have an effect on the applied pressure correction or the annual average volume mixing ratio.

Krasnopolsky [2017] suggests a difference of 1–3%, depending on whether $P_{atm}(t)$ is averaged over sol or over L_S. In this work, we average over L_S, but without the $\omega(L_S)$ correction that *Krasnopolsky* [2017] uses to account for the variable orbital velocity of Mars. There was insufficient pressure data to generate a correction factor as a function of annualized sol. However, the daily pressure averaged over sol using available data indicate that the difference between these two is less than 1% and therefore much less than the uncertainties on the measurements.

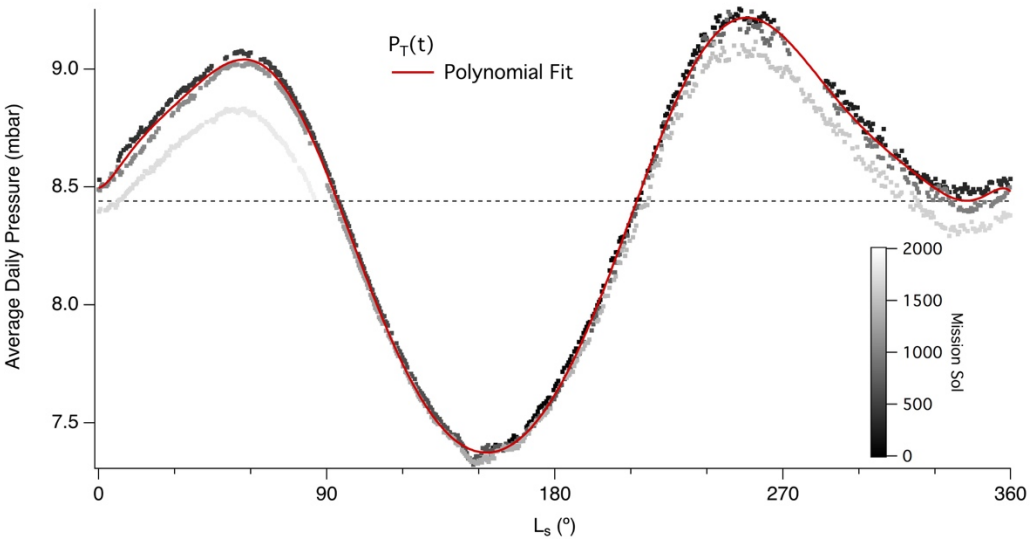

Figure S1. The daily mean pressure values (points, grayscale by mission sol) were fit to a polynomial (red solid line) in order to model the annual pressure curve and develop the correction used for annual average VMR values. The pressure as a function of L_s value was used to calculate a seasonally averaged surface pressure for Gale Crater, is indicated by the horizontal dashed line at 8.46 mbar.

Table S2. Derived correction factor (F_P) for annual average volume mixing ratio (VMR'). *Uploaded as: trainer_table_S2.xlsx*

3. Possible temperature effect on VMR measurements

We investigated the possibility of a sampling bias in the volume mixing ratio determinations correlated with the Mars air temperature at the time of the atmospheric ingestion. This hypothesis was tested to address the concern that the change in temperature between the atmosphere and the ingestion lines of SAM QMS (held at 50°C) could induce a volume expansion, and subsequent mass-dependent fractionation, in which lighter gases could be preferentially lost from the inlet line prior to the valve sealing. For a diagram of the gas flow path during atmospheric experiments see Figure 1 in Franz et al. [2014]. Typical ingestion scripts hold the inlet valve (V28) open for 30s during which such an expansion could take place, thereby skewing the relative mixing ratios of the gases remaining in the manifold and sampled into the QMS.

Because the ratio of $^{40}Ar/^{14}N$ should be held constant during all seasons and atmospheric conditions at the surface, this ratio was used to check for the sampling bias. The data for each individual ingestion are plotted in Figure S2. When the measured $^{40}Ar/^{14}N$ is plotted against the temperature there is a small trend towards a lower ratio at warmer temperatures. In particular, the set of daytime ingestions (Table 1) have an average $^{40}Ar/^{14}N$ that is slightly lower than the nighttime ingestions. The direction of this change is consistent with the possibility of fractionation during sampling as described above, although in general the effect appears minimal as compared to the other uncertainties on the measured value.

3.1 TID 25195 temperature test

As an additional check, an experiment was designed to test for a systematic bias on the derived mixing ratios. The second atmospheric ingestion in TID #25195 on MSL sol 637, L_s 134°, was designed to hold the inlet valve open for 3 minutes while the sample was actively pumped through the manifold by the WRP. This is in comparison to the typical atmospheric ingestion employed until that time, in which the atmospheric sample was passively ingested into the evacuated manifold. The purpose of the experiment was to flush the inlet line and manifold with the cold atmosphere prior to sealing the manifold valves, thus capturing a slug of gas that had minimal time to interact with the inlet heater and manifold heaters prior to isolation. This minimizes the possibility for expansion and fractionation of the atmospheric missing ratios. The resultant $^{40}Ar/^{14}N$ for this ingestion is indicated in Figure S2 with a red diamond. The derived ratio is well within the uncertainty of the ratio obtained during the first ingestion on this sol, in which the standard ingest was employed (open diamond, Figure S2). The similarity of these two measurements and the rest of the lower temperature runs indicates that there is not a significant sampling bias introduced by the elevated manifold temperature. Therefore, although there is a small correlation between the $^{40}Ar/^{14}N$ and air temperature, we cannot prove a causal relationship related to the sampling procedures.

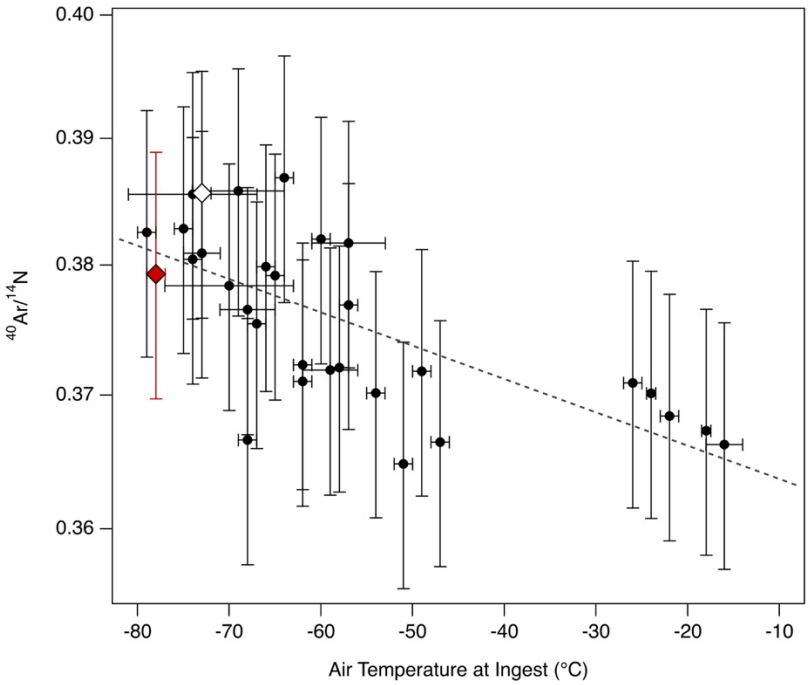

Figure S2. The measured $^{40}Ar/^{14}N$ shows a minor trend with atmospheric temperature at the time of sample ingestion into the SAM QMS, as measured by REMS. The data are grouped into two temperature regimes, based on a nighttime ingestion (colder, left-hand group) as compared to a daytime ingestion (warmer, right-hand group). The line shown has a slope of -0.002 and a correlation coefficient r = -0.69, indicating a moderate relationship with temperature. The data point marked with a red diamond symbol is the second sample ingestion for TID 25195, in which an alternate sampling sequence was used to test for possible instrument temperature effects. The open diamond is the result from the first sample ingestion of the TID 25195 in which the typical sampling sequence was employed.

4. Trends in O_2 corrections over time

We investigated the possibility that the O_2 mixing ratio derivation may be strongly influenced by variations in the corrections applied at *m/z* 32, as discussed in Section 2.1.1. Figure S3. shows the quantification of each of the major contributions to the signal at *m/z* 32. The CO_2 correction (for O_2^+ ion fragments) is fairly stable, showing minor modulation with the changing partial pressure of CO_2 and therefore the seasonal cycle. The background contributions and atmospheric signal are more variable and are discussed in more detail below. Overall, the counts per second (cps) observed at *m/z* 32 has not varied by more than 27% percent over the course of the 5-year mission, and there does not appear to have been a substantial decline in the detector response with time.

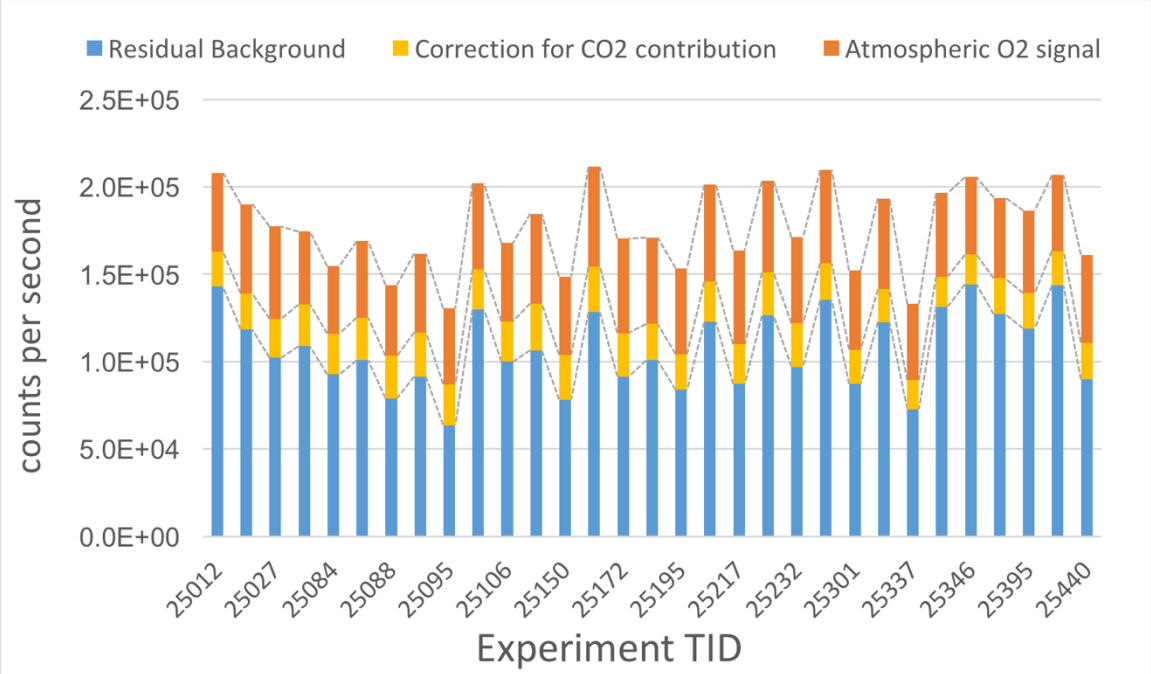

Figure S3. The three contributions to the signal at *m/z* 32 are tracked for each ingestion on Mars. Each column shows the total counts per second observed at *m/z* 32 as a sum of the contributions determined to arise from the presence of residual background gas (bottom, blue), the interference of O_2^+ ions from high partial pressures of CO_2 (middle, yellow), and the atmospheric O_2 signal itself (top, orange).

The relative amplitude of the *m/z* 32 background value is plotted alongside the relative derived O_2 mixing ratio for successive experiments in Figure S4. The background signal shows a clear dependence on whether it is the first or second ingestion within an experiment, which is directly related to the amount of time the manifold has been evacuated prior to measurement in the QMS. Longer evacuation periods lead to lower residual background signals at the *m/z* 32 mass channel, and therefore lower background counts. However, there does not appear to be a correlation between the magnitude of the background signal and the calculated mixing ratio. If the elevated mixing ratios were the result of low background values (and vice versa) there would be an obvious trend in the experiments with two ingestions

mirroring that seen in the background signal. No such trend is observed. The mixing ratio values instead most strongly vary with TID in intervals that are correlated with the annual cycles.

Figure S4. also indicates the relative timing of the solid sample evolved gas analysis (EGA) runs conducted by SAM as they relate to the atmospheric measurements. The background spectra obtained by the instrument prior to the ingestion of should account any residual O_2 in the system from the solid sample analysis, but this check was made to be sure that any contamination did not go unnoticed. The vertical lines in Fig. S4 indicate the individual observations of O2 in EGA runs, and the shading of the bars indicates the strength of the O2 signal (darker = more evolved O_2). The solid sample O_2 data are currently summarized in *Sutter et al.* [2017]. As seen in the plot, the increases in O_2 atmospheric mixing ratio are not uniquely associated with measurements that follow series of EGA runs. In fact, some of the most substantial O_2 releases in EGA experiments are followed by decreases or only minimal increases in measured atmospheric O_2 (e.g., TID 25084 and 25195). We conclude that this is also not a controlling factor in the observed variability of O_2.

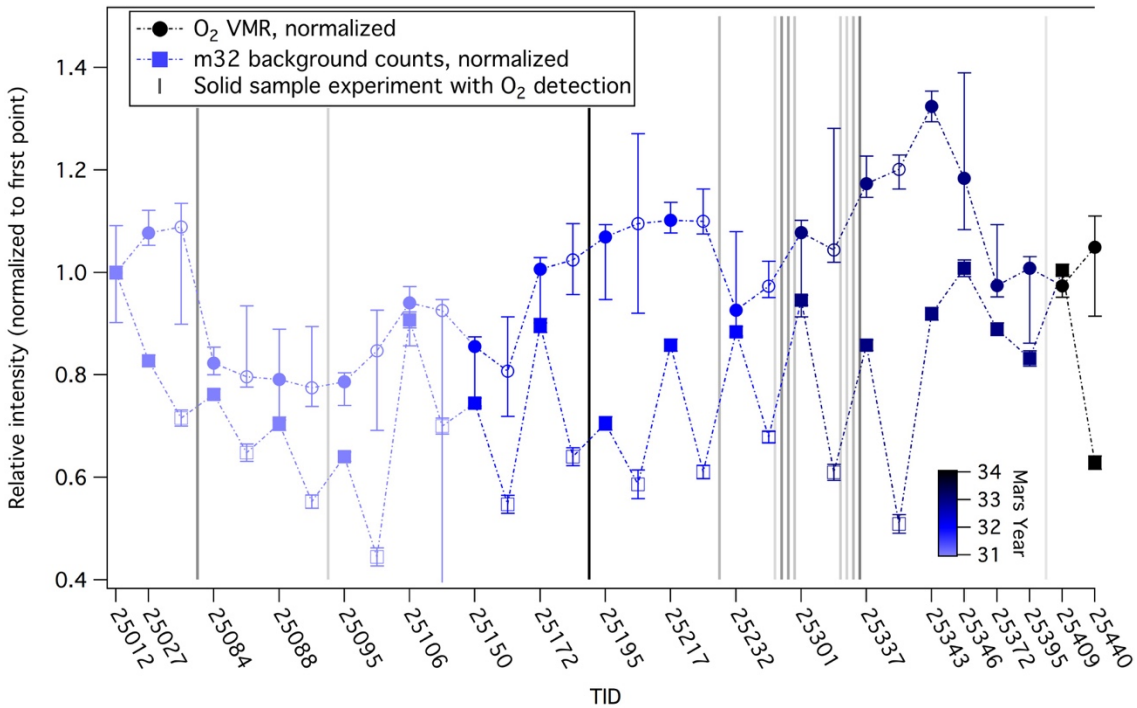

Figure S4. The normalized O_2 mixing ratio (circles) and background counts (squares) for each ingest are plotted against the test ID number (TID). Closed symbols are data from the first ingestion of TID, and open symbols are data from the second ingestion where applicable. Each dataset is normalized to the value of the first atmospheric run on Mars (TID#25012) to highlight the trends over the course of the mission. Points are colored by Mars Year. Vertical bars represent the timing of solid sample evolved gas analyses in which O_2 was detected; the darkness of the gray bars is correlated with the abundance of measured O_2 [*Sutter et al.*, 2017].

5. Argon and Nitrogen corrected for Annual Global Mean Pressure

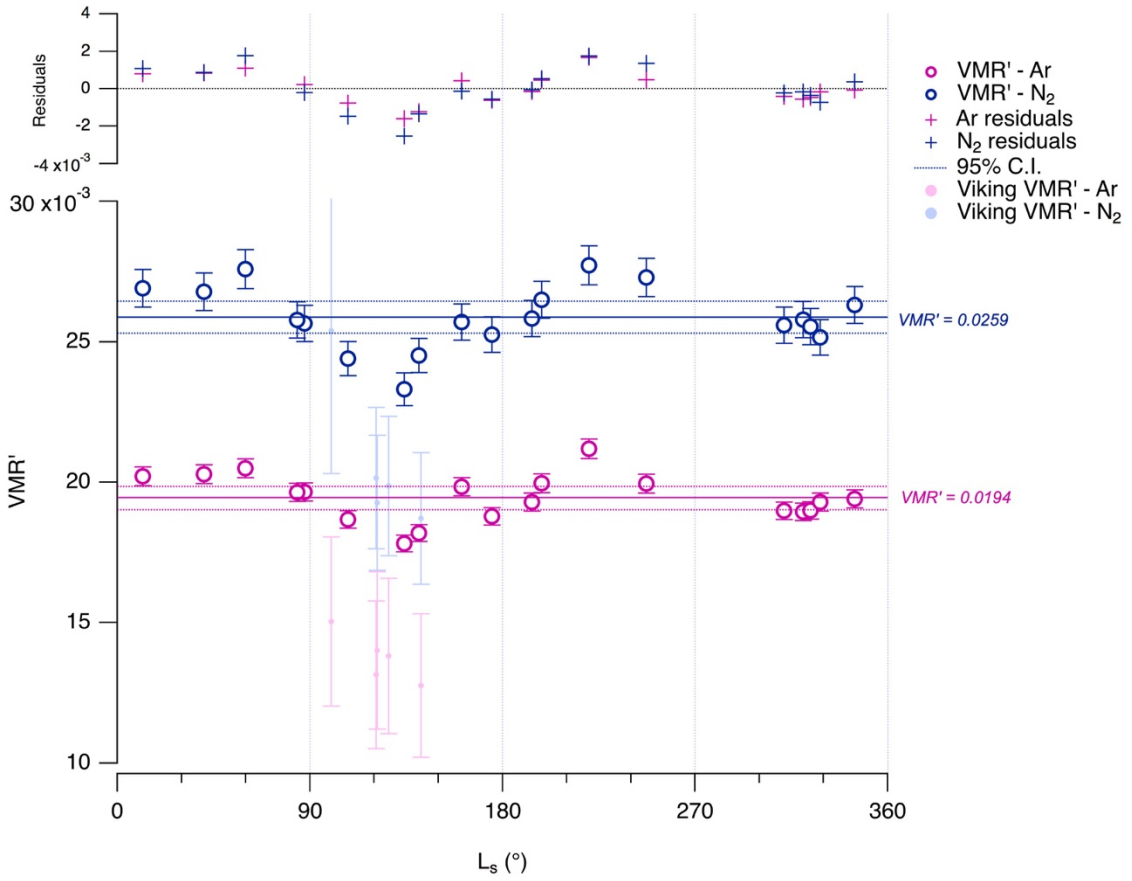

Figure S5. The in situ mixing ratio values for nitrogen (blue) and argon (magenta) were corrected to global mean annual mixing ratios using Equations 5 and S1. Averages for the VMR' values are shown with horizontal solid lines, with ±95% confidence intervals. The top panel shows the residuals between the individual VMR' values and the average. Both corrected N_2 and Ar show deviations from the average outside the indicated uncertainty bands. The measurements made by the Viking GCMS [*Owen et al.*, 1977] and GEX [*Oyama and Berdahl*, 1977] instruments were similarly corrected to VMR', using the Viking Lander pressure curves to develop independent F_P values. These are added to the plot for direct comparison to the SAM data.

The 95% confidence assessment is based on assumption that the corrected volume mixing ratios would be of constant value with normally-distributed errors. The confidence intervals are calculated from measurement scatter. There is an effect based on the uneven sampling cadence (Fig. 1), and the average reported here may not represent the true annual average.

6. Correlations of O_2 concentration with environmental conditions

We tested correlations between O_2 abundance variations with a wide range of environmental parameters, in an attempt to explain the compositional variability. Except for atmospheric dust opacity (Figs. 13(a), S6) and atmospheric UV absorption (Figs. 13(b) and S7), no correlations were observed (Fig. S8). Correlations were tested between the environmental parameters and O_2 VMR, O_2 VMR', and $O_2/^{40}Ar$ ratio. We present the correlations with $O_2/^{40}Ar$ ratio in this section because this quantity eliminates O_2 compositional variability linked to known processes of the CO_2 condensation cycle and associated global transport. The environmental parameters tested were:

- Environmental conditions at the exact time of ingest into SAM (Table 1). These conditions (pressure, ground temperature, air temperature, wind speed, and H_2O humidity) are constrained by the REMS dataset [*Wong et al.*, 2013]. No correlations were found (see Fig. S8(a,d,f,g,i)). Although REM relative humidity values are used for daytime SAM experiments, the REMS values are highly unreliable under conditions of low daytime relative humidity [*Martínez et al.*, 2017].
- Seasonal and inter-annual pressure variation. Instead of the instantaneous pressure at the time of ingest, correlations were tested with the maximum pressure per sol, as constrained by the REMS dataset [*Martínez et al.*, 2017]. No correlations were found (see Fig. S8(e)).
- Seasonal and inter-annual ground temperature variation. Instead of the instantaneous ground temperature at the time of ingest, correlations were tested with the minimum and maximum ground temperature per sol, as constrained by the REMS dataset [*Martínez et al.*, 2017]. No correlations were found (see Fig. S8(b,c)).
- Seasonal and inter-annual humidity variation. Instead of the instantaneous H_2O humidity at the time of ingest, correlations were tested with the maximum H_2O relative humidity measurement per sol, as constrained by the REMS dataset [*Martínez et al.*, 2017]. No correlations were found (see Fig. S8(h)).
- Seasonal and inter-annual dust opacity. Dust opacity was derived from photometric sky imaging from Curiosity's Mastcam [*Smith et al.*, 2016]. Although dust opacity is measured by daytime sky imaging, and most SAM measurements were conducted at night, diurnal variation is minimal outside of the L_S 270° ± 60° season. The potential anticorrelation between dust opacity and $O_2/^{40}Ar$ ratio is discussed in Sec. 4.2 and shown in Figs. 13(a) and S6.
- Seasonal and inter-annual UV absorption in the atmosphere. Ultraviolet absorption was calculated by the model of *Vicente-Retortillo et al.* [2017; 2015], which uses measurements of dust opacity from *Curiosity* and includes geometric effects and variation in UV incident at the top of the atmosphere as a function of L_S. The potential anticorrelation between atmospheric UV absorption and $O_2/^{40}Ar$ ratio is discussed in Sec. 4.2 and shown in Figs. 13(b) and S7.
- CH_4 abundance. Because the SAM/QMS atmospheric VMR experiments were of similar frequency, but generally not obtained at the same times as the CH_4 measurements by SAM /TLS, direct correlation plots could not be generated. Here we include the CH_4 measurements from *Webster et al.* [2018] to plots of O_2/Ar vs. MSL sol in Figs. S6a and S7a. The background seasonal CH_4 data show similar decrease as O_2 in the latter half of each Mars year (Fig. S6a), but the rise of O_2 in the spring occurs earlier and is more variable from year-to-year than the CH_4. The "spike" in CH_4 measured in Mars Year 32 occurred during the same period of time as the relative O_2 enhancement in the Spring

of that year (Fig. S7a). It is possible that there could be a connection, in that similar (unknown) processes may be the source of the O_2 and CH_4 releases. However, without a repeated CH_4 event the following spring such a connection cannot be evaluated with the existing data.

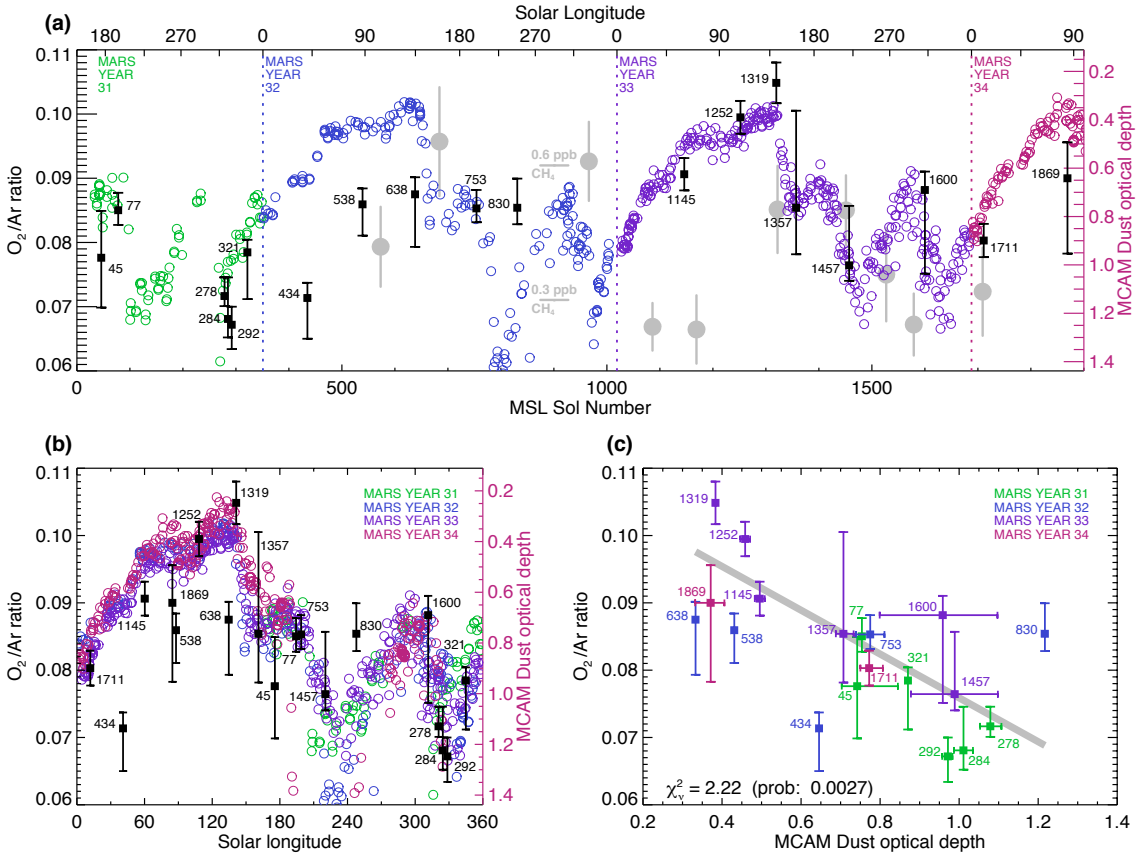

Figure S6. Seasonal variation of the $O_2/^{40}Ar$ ratio suggests a possible anticorrelation with atmospheric dust opacity. **(a)** $O_2/^{40}Ar$ ratios (black squares with sol numbers) are plotted against dust optical depth (colored circles) as a function of MSL mission sol number. Symbol color (and vertical lines) delineate Mars years. The dust opacity axis is reversed to visually emphasize the anticorrelation. SAM/TLS measurements of CH_4 VMR, taken in the high-precision enrichment mode [*Webster et al.*, 2018], are shown in grey with a different vertical scale indicated by horizontal bars near sol 900. **(b)** The same values are plotted against solar longitude (L_S). Mars year is denoted using the same color coding. Despite large variation in dust opacity during the dust storm season (L_S 180°-300°), dust opacity appears to be significantly more repeatable on an annual basis than $O_2/^{40}Ar$ ratio. **(c)** Grey line shows best-fit linear correlation between $O_2/^{40}Ar$ ratio (squares with sol numbers) and dust optical depth. The high χ_ν^2 and probability << 0.1 mean it is not likely there is a simple linear relationship between these quantities, although some relationship is suggested by the data. Panels (a) and (c) suggest that $O_2/^{40}Ar$ ratios in Mars year 32 seem to depart more from a linear relationship with dust opacity than data in MY 31, 33, and 34.

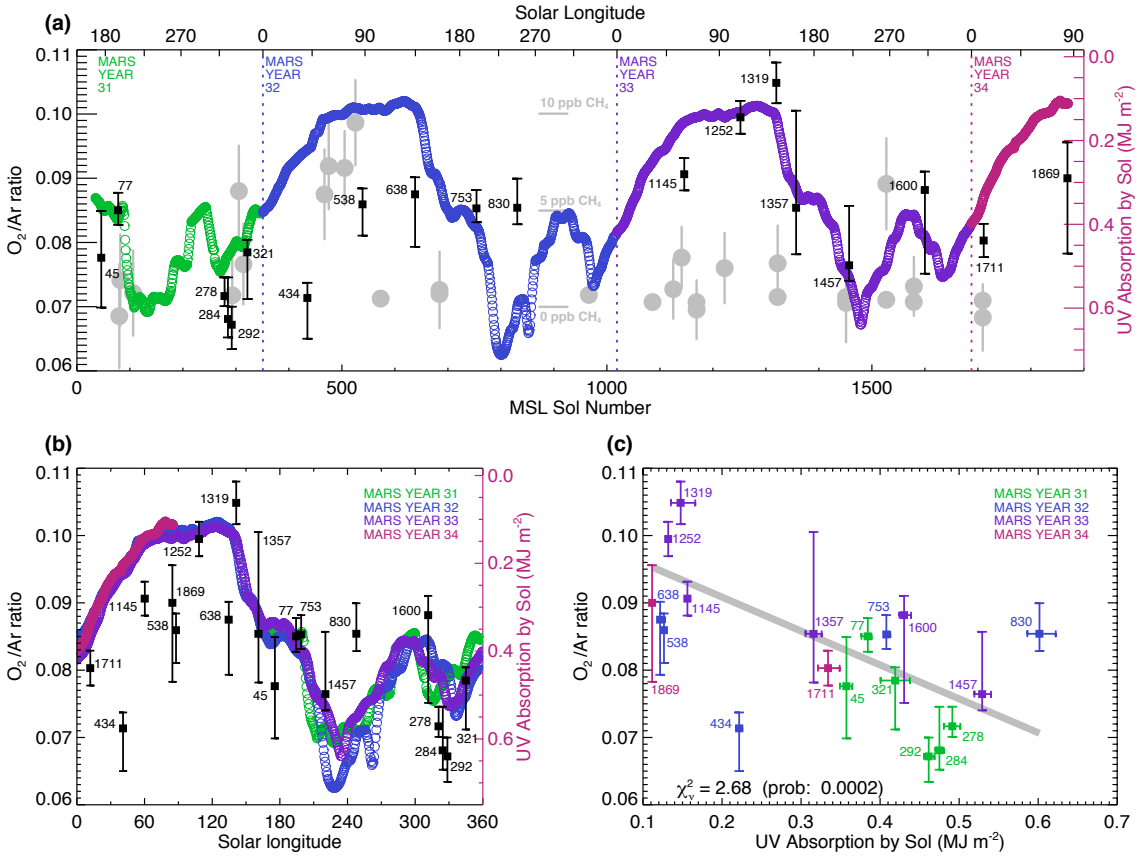

Figure S7. As Fig. S6, but compared with UV atmospheric absorption instead of dust opacity. The SAM/TLS measurements of CH_4 in panel (a) are from both direct and enriched atmospheric samples [*Webster et al.*, 2018]. Absorption energies are integrated over each sol, and derived from the model of *Vicente-Retortillo et al.* [2015].

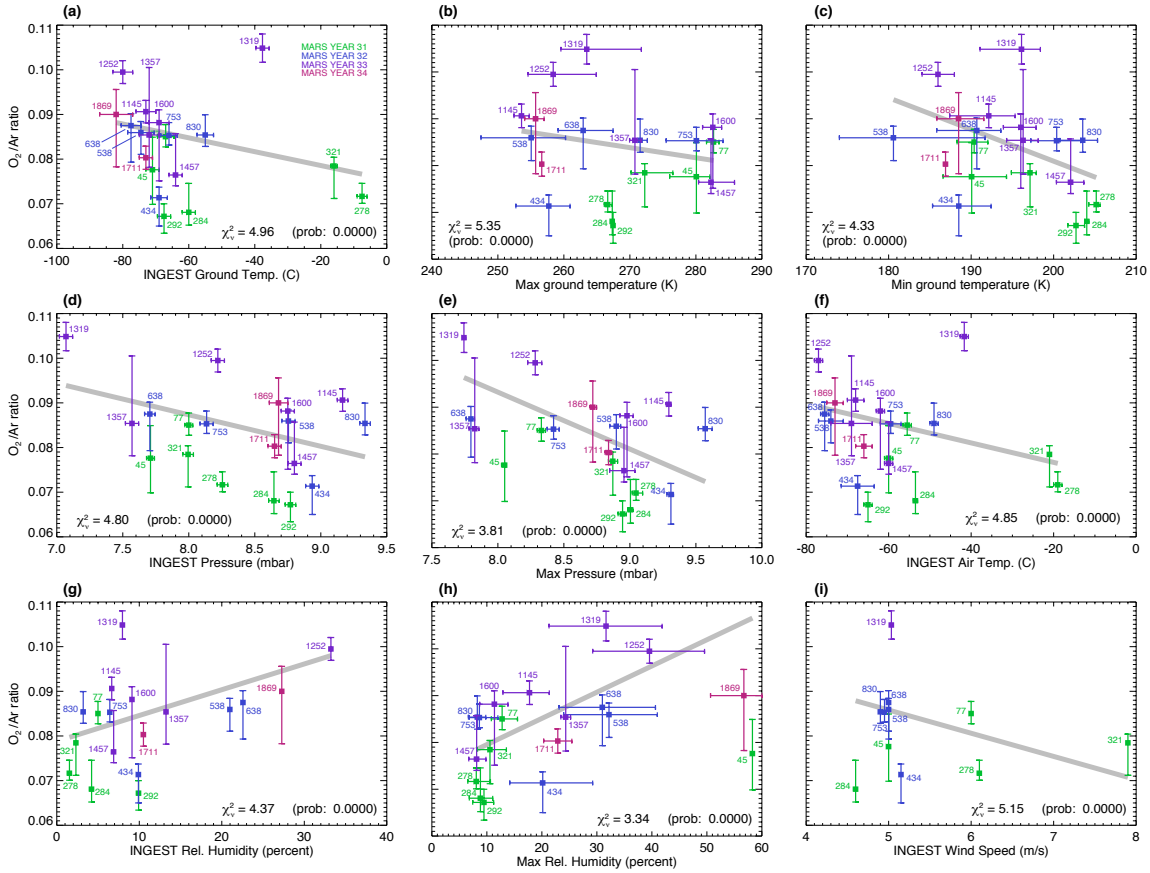

Figure S8. Plots show no significant linear correlation between the O_2/Ar ratio (y-axis) and multiple environmental variables constrained by REMS measurements: **(a)** ground temperature at the time of SAM atmospheric sample ingest; **(b)** maximum and **(c)** minimum daily ground temperature over the MSL mission; **(d)** pressure at time of ingest; **(e)** maximum daily pressure; **(f)** air temperature at time of ingest; **(g)** relative humidity at time of ingest; **(h)** maximum daily relative humidity; and **(i)** wind speed at time of ingest. Determination of environmental conditions at time of SAM ingest (a,d,f,g,i) are based on REMS MODRDR version 6 level 4 data products, but the process is otherwise as described in *Wong et al.* [2013]. Determination of seasonal pressure, relative humidity, and ground temperature values from REMS data (b,c,e,h) are described in *Martínez et al.* [2017].

References

Franz, H. B., et al. (2017), Initial SAM calibration gas experiments on Mars: Quadrupole mass spectrometer results and implications, *Planet. Space Sci.*, *138*, 44-54, doi:10.1016/j.pss.2017.01.014.

Franz, H. B., et al. (2014), Analytical Techniques for Retrieval of Atmospheric Gas Abundances and Isotope Ratios Measured by the Quadrupole Mass Spectrometer of the Sample Analysis at Mars Instrument Suite on Mars Science Laboratory, *Planet. Space Sci.*, *96*, 99-113, doi:10.1016/j.pss.2014.03.005.

Krasnopolsky, V. A. (2017), Annual mean mixing ratios of N_2, Ar, O_2, and CO in the martian atmosphere, *Planet. Space Sci.*, *144*, 71-73, doi:10.1016/j.pss.2017.05.009.

Martínez, G. M., et al. (2017), The Modern Near-Surface Martian Climate: A Review of In-situ Meteorological Data from Viking to Curiosity, *Space Sci. Rev.*, *212*(1), 295-338, doi:10.1007/s11214-017-0360-x.

Owen, T., K. Biemann, D. R. Rushneck, J. E. Biller, D. W. Howarth, and A. L. Lafleur (1977), The composition of the atmosphere at the surface of Mars, *J. Geophys. Res.*, *82*(28), 4635-4639, doi:10.1029/JS082i028p04635.

Oyama, V. I., and B. J. Berdahl (1977), The Viking Gas Exchange Experiment results from Chryse and Utopia surface samples, *J. Geophys. Res.*, *82*(28), 4669-4676, doi:10.1029/JS082i028p04669.

Smith, M. D., M. P. Zorzano, M. Lemmon, J. Martin-Torres, and T. M. de Cal (2016), Aerosol optical depth as observed by the Mars Science Laboratory REMS UV photodiodes, *Icarus*, *280*, 234-248, doi:10.1016/j.icarus.2016.07.012.

Sutter, B., et al. (2017), Evolved gas analyses of sedimentary rocks and eolian sediment in Gale Crater, Mars: Results of the Curiosity rover's sample analysis at Mars instrument from Yellowknife Bay to the Namib Dune, *J. Geophys. Res.*, *122*(12), 2574-2609, doi:10.1002/2016je005225.

Trainer, M. G. (2019), Volume Mixing Ratios of Major Atmospheric Components on Mars as Measured by MSL/SAM, edited, doi:https://doi.org/10.7910/DVN/CVUOWW.

Vicente-Retortillo, Á., G. M. Martínez, N. O. Renno, M. T. Lemmon, and M. de la Torre-Juárez (2017), Determination ofdust aerosol particle size at GaleCrater using REMS UVS and Mastcam measurements, *Geophys. Res. Lett.*, *44*, 3502-3508, doi:10.1002/2017GL072589.

Vicente-Retortillo, A., F. Valero, L. Vazquez, and G. M. Martinez (2015), A model to calculate solar radiation fluxes on the Martian surface, *J. Space Weather Space Clim.*, *5*, 13, doi:10.1051/swsc/2015035.

Webster, C. R., et al. (2018), Background levels of methane in Mars' atmosphere show strong seasonal variations, *Science*, *360*(6393), 1093-+, doi:10.1126/science.aaq0131.

Wong, M. H., et al. (2013), MSL/REMS Measurements of Conditions During MSL/SAM Atmospheric Ingestion Events, paper presented at 44th Lunar and Planetary Science Conference, LPI Contribution No. 1719, The Woodlands, TX.